

Multilevel and Sequential Monte Carlo for Training-Free Diffusion Guidance

Aidan Gleich¹ Scott C. Schmidler¹

Abstract

We address the problem of accurate, training-free guidance for conditional generation in trained diffusion models. Existing methods typically rely on point-estimates to approximate the posterior score, often resulting in biased approximations that fail to capture multimodality inherent to the reverse process of diffusion models. We propose a sequential Monte Carlo (SMC) framework that constructs an unbiased estimator of $p_\theta(y|x_t)$ by integrating over the full denoising distribution via Monte Carlo approximation. To ensure computational tractability, we incorporate variance-reduction schemes based on Multi-Level Monte Carlo (MLMC). Our approach achieves new state-of-the-art results for training-free guidance on CIFAR-10 class-conditional generation, achieving 95.6% accuracy with $3\times$ lower cost-per-success than baselines. On ImageNet, our algorithm achieves $1.5\times$ cost-per-success advantage over existing methods.

1. Introduction

Diffusion models have emerged as a leading methodology for generative modeling (Sohl-Dickstein et al., 2015; Ho et al., 2020; Song & Ermon, 2019; Song et al., 2021). They are capable of generating high-quality samples across a range of domains, including images (Nichol & Dhariwal, 2021; Rombach et al., 2022), audio (Kong et al., 2021), molecules (Hoogeboom et al., 2022), and text (Li et al., 2022). A learned model $p_\theta(x_0)$ targets the true data distribution $p(x_0)$, enabling unconditional sampling from complex, high-dimensional distributions.

In many applications, however, the goal is not to sample from the distribution $p(x_0)$ but instead the conditional distribution $p(x_0|y)$, where y is information such as an image

¹Department of Statistical Science, Duke University, Durham, North Carolina. Correspondence to: Aidan Gleich <aidan.gleich@duke.edu>.

label or molecule property. Given a likelihood function $p(y|x_0)$ (e.g. a classifier), this conditional distribution can be written in terms of the generative model using Bayes' rule: $p_\theta(x_0|y) \propto p_\theta(x_0)p(y|x_0)$. Efficient conditional sampling via diffusion models remains a central focus of the literature, with numerous approaches proposed in a variety of contexts.

Some approaches, particularly in image generation, include conditional information directly during training (Ho & Salimans, 2022) or train auxiliary classifiers to guide the sampling process (Dhariwal & Nichol, 2021). While effective, these methods incur high computational costs during training and limit model flexibility; adapting to a new likelihood $p(y|x_0)$ requires retraining.

To address this inflexibility, a separate line of work focuses on *training-free guidance*. These methods combine a pre-trained unconditional model $p_\theta(x_0)$ with approximations to the posterior score $\nabla_{x_t} \log p_\theta(y|x_t)$. Diffusion Posterior Sampling (DPS) (Chung et al., 2023) pioneered this approach by approximating the intractable marginal likelihood $p_\theta(y|x_t)$ with a point estimate $p(y|\hat{x}_\theta(x_t))$, effectively collapsing the posterior to a Dirac mass at the conditional mean. Subsequent methods, including LGD (Song et al., 2023), FreeDoM (Yu et al., 2023), and Universal Guidance (Bansal et al., 2024), refine this approach through Monte Carlo sampling over Gaussian kernels, recurrent denoising strategies, and energy-based optimization. Ye et al. (2024) unifies these methods into a common hyperparameter framework. However, they all rely on point approximations that fail to capture the multimodality of the posterior distribution $p_\theta(x_0|x_t)$, introducing bias that accumulates over the diffusion trajectory.

The Twisted Diffusion Sampler (TDS) (Wu et al., 2023) offers a theoretically distinct formulation, framing conditional sampling as Sequential Monte Carlo (SMC) with learned “twisting functions” to approximate the optimal proposal distribution. While this SMC perspective provides asymptotic exactness in principle, practical implementations of TDS construct their twisting functions using the same point estimate approximations discussed above. Consequently, TDS inherits the fundamental limitation of heuristic guidance: it fails to integrate over the full posterior $p_\theta(x_0|x_t)$ in the

proposal step, leading to weight degeneracy in multimodal settings.

To address these shortcomings, we propose an SMC framework to sample from conditional distributions using only a pre-trained unconditional model. Unlike biased heuristics that approximate the score guidance term, our approach targets the exact conditional distribution by utilizing an unbiased estimator of the marginal likelihood $p_\theta(y|x_t)$. To render this estimator computationally tractable, we employ a Multilevel Monte Carlo (MLMC) scheme that integrates over the full denoising distribution $p_\theta(x_0|x_t)$. Our contributions are threefold: (1) we formulate a sequential Monte Carlo framework that leverages unbiased likelihood estimators to target the exact conditional distribution, enabling the rigorous correction of biased heuristics; (2) we extend the MLMC framework of [Shaw et al. \(2025\)](#) to the training-free guidance problem, reducing the variance of likelihood estimates at a fraction of the cost of naive Monte Carlo; and (3) we demonstrate state-of-the-art performance: on CIFAR-10, our method achieves 95.6% accuracy, surpassing existing training-free baselines.

Critically, our approach achieves superior computational efficiency when measured by cost-per-success—the expected cost to generate at least one valid conditional sample. On CIFAR-10, our method requires only 23s to generate a valid sample with 95.6% probability, while baselines require 5 runs at 13.7s each to achieve comparable success probability. This $3\times$ efficiency advantage, combined with state-of-the-art guidance validity, demonstrates that unbiased estimation is not just theoretically principled but also practically superior on the problem.

2. Background

2.1. Diffusion Models

A diffusion model is a generative model trained to sample from an unknown distribution $p(x_0)$ represented by a finite set of samples x_0^1, \dots, x_0^n . It does so by reversing a predefined forward process that iteratively noises data points via a Markov chain $q(x_t|x_{t-1})$. The Markov chain is defined such that by time T the noised data approximately follows a simple distribution, such as a standard Gaussian.

In the Denoising Diffusion Probabilistic Model (DDPM) formulation ([Ho et al., 2020](#)), this forward process is defined by a finite sequence of time steps $t \in \{1, \dots, T\}$ as $q(x_t|x_{t-1}) = \mathcal{N}(x_t; \sqrt{\alpha_t}x_{t-1}, (1 - \alpha_t)\mathbf{I})$, where the parameters $\{\alpha_t\}_{t=1}^T$ control the noise level of the forward process. Noised data points can then be sampled from the forward process in a single step:

$$q(x_t|x_0) = \mathcal{N}(x_t; \sqrt{\alpha_t}x_0, (1 - \alpha_t)\mathbf{I})$$

where $\bar{\alpha}_t = \prod_{i=1}^t \alpha_i$, and these samples are used to train a

neural network $\epsilon_\theta(x_t, t)$ to predict the noise component ϵ of $x_t = \sqrt{\bar{\alpha}_t}x_0 + \sqrt{1 - \bar{\alpha}_t}\epsilon$. Via Tweedie's formula, this also yields an estimate of the score of the marginal $q_t(x_t)$ of the forward process ([Song & Ermon, 2019](#)). We denote the implied score network as $s_\theta(x_t, t) := -\epsilon_\theta(x_t, t)/\sqrt{1 - \bar{\alpha}_t} \approx \nabla_{x_t} \log q(x_t)$.

The network $\epsilon_\theta(x_t, t)$ is then used to define the reverse process $p_\theta(x_{t-1}|x_t)$. This learned process is trained to approximate the forward process $q(x_{t-1}|x_t, x_0)$, which is a tractable Gaussian when conditioned on x_0 . Typically, the reverse process is also defined as Gaussian:

$$p_\theta(x_{t-1}|x_t) = \mathcal{N}(x_{t-1}; \mu_\theta(x_t, t), \sigma_t^2 \mathbf{I}).$$

A crucial insight from ([Ho et al., 2020](#)) is that $\mu_\theta(x_t, t)$ can be predicted directly from the denoising network $\epsilon_\theta(x_t, t)$:

$$\mu_\theta(x_t, t) = \frac{1}{\sqrt{\alpha_t}} \left(x_t - \frac{1 - \alpha_t}{\sqrt{1 - \bar{\alpha}_t}} \epsilon_\theta(x_t, t) \right).$$

The generative model is then given by

$$p_\theta(x_0) = \int p(x_T) \prod_{t=1}^T p_\theta(x_{t-1}|x_t) dx_{1:T}.$$

Thus once ϵ_θ has been fit, choosing T such that x_T is approximately $\mathcal{N}(0, \mathbf{I})$ enables sampling from this model by drawing x_T from a standard normal distribution and iterating through the reverse kernels $p_\theta(x_{t-1}|x_t)$.

2.2. Sequential Monte Carlo

Sequential Monte Carlo (SMC) methods are a broad class of algorithms designed to sample from complex target distributions $\pi(x)$ ([Del Moral et al., 2006](#)). For our purposes, SMC can be viewed as a generalization of importance sampling: the target distribution is represented by a set of N weighted particles $\{x^{(i)}, w^{(i)}\}_{i=1}^N$ generated by the algorithm. The sampler is typically constructed by defining a sequence of distributions $\mu_0, \dots, \mu_{V-1}, \mu_V$ that terminates in the target distribution ($\mu_V = \pi$). The sequence is chosen such that μ_0 is easy to sample from and μ_v is “close” to μ_{v+1} . Sampling proceeds by drawing a set of initial particles from the distribution μ_0 . Each step of the algorithm begins with particles $\{x_{v-1}^{(i)}\}_{i=1}^N$ distributed approximately according to μ_{v-1} . The algorithm then performs three steps:

- Propagate:** Particles are moved via a proposal distribution
- Reweight:** Particles are assigned an importance weight $w_v^{(i)} = \frac{\mu_v(x_v^{(i)})}{\mu_{v-1}(x_{v-1}^{(i)})r_v(x_v^{(i)}|x_{v-1})}$ to correct for the proposal.

3. **Resample:** A new set $\{x_v^{(i)}\}_{i=1}^N$ is sampled with replacement from the weighted particles, yielding an unweighted approximation of μ_v .

Each step can be viewed as sampling/importance resampling (SIR) (Rubin, 1987) with target distribution μ_v . As $N \rightarrow \infty$, the empirical measure formed by the resampled particles provides a consistent estimator of the target distribution μ_v .

2.3. Diffusion as SMC

As noted by Wu et al. (2023), the reverse process of the diffusion model can be reformulated as an SMC algorithm by setting the number of SMC steps equal to the number of diffusion steps T and aligning the sequence of target distributions $\{\mu_t\}_{t=T}^0$ with the marginal distributions of the reverse process $p_\theta(x_t)$ at the finite set of times $t \in \{0, \dots, T\}$. The resulting SMC algorithm has target distributions that exactly mirror the reverse process of the diffusion model (Trippe et al., 2023; Cardoso et al., 2024; Wu et al., 2023). Sampling begins by drawing *i.i.d.* particles from initial distribution $\mu_T = p(x_T) = N(x_T; 0, \mathbf{I})$. Proposal distributions are given by the trained reverse process: $r_t(x_{t-1}|x_t) = p_\theta(x_{t-1}|x_t)$. In the absence of conditioning information, the proposals target the desired (approximate) distribution by construction, the importance weights are uniform, and the reweighting and resampling steps of the SMC algorithm can be omitted.

3. Conditional Diffusion Sampling Via SMC

Given a diffusion model $p_\theta(x_0)$ estimated to approximate target $p(x_0)$ and a “likelihood” function $p(y|x_0)$ for observed information y on which we wish to condition, defined over the support of $p(x_0)$, our goal is to sample from the conditional distribution $p_\theta(x_0|y) \propto p_\theta(x_0)p(y|x_0)$ (as an approximation to $p(x_0|y) \propto p(x_0)p(y|x_0)$) without additional training.

A naive approach uses the unconditional diffusion model reverse process to generate samples from $p_\theta(x_0)$, which can then be reweighted according to the likelihood function $w_0^{(i)} \propto p(y|x_0^{(i)})$ and resampled. This defines a simplistic SMC algorithm, equivalent to sampling-importance-resampling (SIR (Rubin, 1987)) with proposal distribution $p_\theta(x_0)$ and target distribution $p_\theta(x_0|y)$. However, $p_\theta(x_0)$ may be far from $p_\theta(x_0|y)$ (e.g. in KL divergence, which determines sample size requirements (Chatterjee & Diaconis, 2018) for importance sampling), which can result in a low probability of generating a sample value x_0 from a high-density region of $p_\theta(x_0|y)$. For example, if the condition is a hard constraint (e.g. $p(y|x_0) \in \{0, 1\}$ indicates class membership or subvector agreement), the probability of sampling a valid x_0 is given by the marginal probability $p_\theta(y) = \int p(y|x_0)p_\theta(x_0)dx_0$. In high dimensions where

$p_\theta(y)$ may be exponentially small, this naive approach is impractical. This problem arises due to the attempt to move particles from $p_\theta(x_0)$ to $p_\theta(x_0|y)$ in a single step.

To address this, it is preferred to choose the sequence of intermediate distributions to ensure that μ_t is close to μ_{t+1} for all t . A natural choice is to condition the reverse steps of the diffusion model, setting $\mu_t = p_\theta(x_t|x_{t+1}, y)$ (Whiteley & Lee, 2014; Wu et al., 2023). If these conditional distributions can be sampled exactly then reweighting/resampling are not required, and the resulting samples are drawn exactly from the target distribution with only a single particle by the chain rule of probability. However, sampling from $p_\theta(x_t|x_{t+1}, y)$ requires knowledge of the intractable marginal likelihood $p_\theta(y|x_t)$. Accurately approximating this quantity is essential for effective conditional sampling and will be a central challenge we address.

3.1. Conditional Reverse Steps and Marginal Likelihoods

Many existing *training-free guidance* methods (Chung et al., 2023; Song et al., 2023; Ye et al., 2024) attempt to sample approximately from $p_\theta(x_t|x_{t+1}, y)$ by approximating the score of the conditional reverse process $p_\theta(x_t|y)$ by

$$\begin{aligned} \nabla_{x_t} \log p_\theta(x_t|y) &= \nabla_{x_t} \log p_\theta(x_t) + \nabla_{x_t} \log p_\theta(y|x_t) \\ &\approx s_\theta(x_t, t) + \tilde{s}_\theta(x_t, y, t) \end{aligned} \quad (1)$$

to enable score-based guidance using the unconditional score model combined with an approximation $\tilde{s}_\theta(x_t, y, t)$ to $\nabla_{x_t} \log p_\theta(y|x_t)$. The difficulty is that $p_\theta(y|x_t)$ is intractable, requiring marginalization over x_0, x_1, \dots, x_{t-1} :

$$p_\theta(y|x_t) = \int p(y|x_0)p_\theta(x_{0:t-1}|x_t)dx_{0:t-1}.$$

Diffusion posterior sampling (DPS) (Chung et al., 2023) addresses this problem by applying the approximation $\tilde{s}_\theta(x_t, y, t) = \nabla_{x_t} \log \tilde{p}(y|x_t)$ with

$$p_\theta(y|x_t) \approx \tilde{p}(y|x_t) := p_\theta(y|\hat{x}_\theta(x_t, t)) \quad (2)$$

where $\hat{x}_\theta(x_t) \approx \mathbb{E}[x_0|x_t]$ is produced by the denoising network. This approximation replaces the full conditional distribution $p_\theta(x_0|x_t)$ with a Dirac measure $\delta_{\hat{x}_\theta(x_t)}(x_0)$ at its (approximated) expected value. Wu et al. (2023) combine (1) and (2) to form a proposal distribution for SMC.

As noted in (Song et al., 2023), this approximation can severely underestimate uncertainty in the distribution $p_\theta(x_0|x_t)$. For moderate to large t , this distribution is almost certainly multimodal if the underlying data distribution $p(x_0)$ is; this will be the case if, for example, the unconditional target distribution $p_0(x)$ is a mixture of class-conditional densities. For multimodal distributions, the expectation is typically a poor location parameter, and the

point measure $\delta_{\hat{x}_\theta(x_t)}(x_0)$ will be a particularly poor approximation of the distribution, resulting in the targeted sequence of marginal distributions $\tilde{p}_\theta(x_t | y) \propto p_\theta(x_t) \tilde{p}_\theta(y | x_t)$ diverging from the true marginals $p_\theta(x_t | y)$ (see Appendix A.2). This is because the approximation shifts mass towards regions where the likelihood at the expected state $p(y | \mathbb{E}[x_0 | x_t])$ is maximized, driving the trajectory too strongly towards the mode and ignoring uncertainty in the conditional distribution $p_\theta(x_0 | x_t)$.

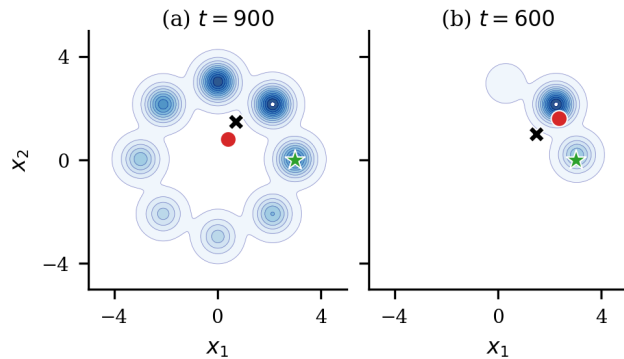


Figure 1. Posterior distribution $p(x_0 | x_t)$ for an 8-component ring GMM. Contours show $p(x_0 | x_t)$; \times marks the noisy observation x_t ; \bullet shows the point estimate $\mathbb{E}[x_0 | x_t]$; \star indicates the true x_0 . (a) At high noise ($t = 900$), the posterior is multimodal and the point estimate lies in a low-density region at the center of the ring. (b) At moderate noise ($t = 600$), the mass concentrates on two modes and the point estimate lies near the non-target mode.

Figure 1 demonstrates this effect for $p(x_0)$ given by an 8 component Gaussian mixture model (GMM). Calculation of $p_\theta(y | x_t) = \int p(y | x_0) p_\theta(x_0 | x_t) dx_0$ requires integrating over the conditional distribution $p_\theta(x_0 | x_t)$. As seen in Figure 1, when this distribution is multimodal approximating this integral by replacing $p_\theta(x_0 | x_t)$ with a point estimate can lead to significant bias. Despite x_0 being the mode of the target distribution, the mean $\mathbb{E}[x_0 | x_t]$ lands in areas of low-density or non-target modes, both of which cause $p(y | \mathbb{E}[x_0 | x_t])$ to estimate $p(y | x_t)$ poorly (see Appendix A.3).

The point estimator faces further limitations when $p(y | x_0) \propto 1_{A_y}$ for some $A_y \subset \mathcal{X}$ (e.g. inpainting (Lugmayr et al., 2022)). In this case, $p_\theta(y | x_t) = p_\theta(x_0 \in A_y | x_t)$ is the probability of x_0 lying in A_y given x_t ; for large t this approaches the marginal: $p_\theta(x_0 \in A_y | x_t) \approx p_\theta(x_0 \in A_y)$. If the set A_y has low probability under the (approximated) data distribution $p_\theta(x_0)$, the mean estimate $\hat{x}_\theta(x_t)$ is unlikely to lie within A_y for large t , causing $p(A_y | \hat{x}_\theta(x_t))$ to incorrectly estimate the probability as 0.

3.2. Monte Carlo Approximation to Marginal Likelihoods

To overcome the limitations of DPS-style methods illustrated above, we instead estimate $p_\theta(y | x_t)$ directly by Monte Carlo integration. A simple MC approximation can be obtained by drawing samples $x_{0|t}^{(1)}, \dots, x_{0|t}^{(m)} \sim p_\theta(x_0 | x_t)$ via the unconditional diffusion model, and forming the estimator

$$\hat{p}_\theta(y | x_t) = \frac{1}{m} \sum_{i=1}^m p(y | x_{0|t}^{(i)}). \quad (3)$$

Unlike the approximation $\tilde{p}(y | x_t)$ in (2), \hat{p} is an unbiased and consistent estimator of $p_\theta(y | x_t)$, and straightforward bounds on the Monte Carlo approximation error allow m to be chosen to achieve desired accuracy.

However, this comes at significant cost, as samples from $p_\theta(x_0 | x_t)$ require evaluations of the reverse process of the generative model. In addition, the efficiency of this estimator depends critically on the (approximated) data distribution $p_\theta(x_0)$ and also on the form of $p(y | x_0)$. For example, when $p(y | x_0) \propto 1_{A_y}(x_0)$ (inpainting), the required sample size m is determined by $p_\theta(A_y | x_t)$, which for large t is approximately $p_\theta(x_0 \in A_y) =: p_{A_y}$. If p_{A_y} is small, this creates a rare-event estimation problem: naive MC estimation by drawing from $p_\theta(x_0)$ will require $m \geq \frac{1}{p_{A_y} \delta \epsilon^2}$ samples to achieve relative approximation accuracy ϵ with probability δ , i.e. $\Pr(|\hat{p}_A - p_A| > p_A \epsilon) \leq \delta$. Using the full reverse process schedule of the unconditional model, each timestep t requires $O(mt)$ calculations per particle for a cost of $O(mT^2)$ to guide a single particle. To address this, we propose a more efficient MC estimator in Section 3.3.1

Song et al. (2023) also employ Monte Carlo integration to approximate $p_\theta(y | x_t)$, but do not sample from $p_\theta(x_0 | x_t)$ via the reverse process, instead using a Gaussian approximation centered at $\hat{x}_\theta(x_t)$. This approximation, while lower cost, fails to capture the multimodality of $p_\theta(x_0 | x_t)$ discussed above, resulting in a biased estimator. In contrast, our approach yields an unbiased estimate of $p_\theta(y | x_t)$, at the cost of additional computation—a cost we mitigate through MLMC (Section 3.3.1).

3.3. Sequential Monte Carlo Sampler

We leverage $\hat{p}_\theta(y | x_t)$ to construct an SMC sampler targeting the conditional distribution $p_\theta(x_0 | y)$. Particles are propagated by a proposal distribution $r_t(x_{t-1} | x_t, y)$ and reweighted to correct for discrepancies between the proposal distribution and the true reverse conditional process. The resulting SMC algorithm is initialized by drawing particles $\{x_T^{(i)}\}_{i=1}^N \sim \mathcal{N}(\mathbf{0}, \mathbf{I})$. Then for each time step t , the sampler performs two operations:

1. **Proposal:** Each particle $x_{t+1}^{(i)}$ from the previous step is propagated using a proposal distribution $r_t(x_t | x_{t+1}^{(i)}, y)$.
2. **Weight & Resample:** Compute an importance weight for each particle by calculating the approximation $\hat{p}_\theta(y | x_t)$ and forming

$$w_t^{(i)} = \frac{\hat{p}_\theta(y | x_t) p_\theta(x_t | x_{t+1}^{(i)})}{\hat{p}_\theta(y | x_{t+1}) r_t(x_t | x_{t+1}, y)}.$$

Particles are then resampled with probabilities proportional to their weights.

The approximation $\hat{p}_\theta(y | x_t)$ also implies an approximate $\hat{\nabla}_{x_t} p_\theta(y | x_t)$ suitable for use in (1); however, calculation of $\hat{\nabla}_{x_t} p_\theta(y | x_t)$ requires computing pathwise derivatives through the stochastic reverse process, which is numerically unstable and prohibitively memory-intensive. We thus use the estimate $\hat{p}_\theta(y | x_t)$ directly within a weighting and resampling scheme, avoiding the need to modify the proposal distribution via unstable score approximations.

Because $\hat{p}_\theta(y | x_t)$ is an unbiased estimate of $p_\theta(y | x_t)$, marginally the particles follow the distribution of the conditional reverse process $p_\theta(x_t | x_{t+1}, y)$. This contrasts with the Twisted Diffusion Sampler (TDS) (Wu et al., 2023), which also employs an SMC framework, with importance weights constructed using the point estimate $p(y | \hat{x}_\theta(x_t, t))$ discussed in Section 3.1. The resulting marginal distributions of the TDS particles can diverge from the true conditionals $p_\theta(x_t | x_{t+1}, y)$ especially when $p_\theta(x_0 | x_t)$ is multimodal. This in turn can lead to extreme weight variability at the final resampling step; Wu et al. (2023) report this in the form of Effective Sample Size (ESS) collapse on MNIST and CIFAR-10. In contrast, our method maintains a stable ESS as seen in Figure 2b.

3.3.1. MLMC FOR MARGINAL LIKELIHOOD

To address the computational cost of sampling from $p_\theta(x_0 | x_t)$, we introduce a multilevel Monte Carlo (MLMC) approach (Giles, 2008; Blanchet et al., 2019); MLMC has also recently been applied to diffusion modeling by Shaw et al. (2025). We first define a hierarchy of discretized reverse processes $\{p_\theta^{(\ell)}(\cdot | x_t)\}_{\ell=0}^L$ with step sizes $h_\ell = h_0 M^{-\ell}$, where h_0 is the base step size and M is an integer refinement factor (Giles, 2008). Alternatively, the number of reverse steps T_0 at level 0 and the refinement factor M imply the number of levels $L = \log_M (T/T_0)$. Simulating the reverse process at a coarser level $\ell' < \ell$ requires fewer neural function evaluations (NFEs); however, the resulting samples $x_0^{(\ell')} \sim p_\theta^{(\ell')}(\cdot | x_t)$ are drawn from a different marginal distribution than the target $p_\theta(\cdot | x_t)$ due to the introduction of discretization bias. MLMC corrects for this bias by decomposing $\mathbb{E}_{x_0 \sim p_\theta(x_0 | x_t)}[p(y | x_0)]$ into a telescoping sum

of expected differences between successive discretization levels:

$$\mathbb{E}[p(y | x_0^{(L)})] = \mathbb{E}[p(y | x_0^{(0)})] + \sum_{\ell=1}^L \mathbb{E} \left[p(y | x_0^{(\ell)}) - p(y | x_0^{(\ell-1)}) \right]. \quad (4)$$

The MLMC estimator leverages computationally cheap samples obtained at large step-sizes, while reserving the use of fewer, more expensive, finer step-size simulations to estimate incremental corrections. The first term is estimated using N_0 samples from the base (coarsest) model, with subsequent terms estimated using N_ℓ coupled pairs of samples to approximate the expected difference between discretization levels. The computational efficiency of MLMC relies on the variance of these corrections $V_\ell = \mathbb{V}[p(y | x_0^{(\ell)}) - p(y | x_0^{(\ell-1)})]$ decaying rapidly as ℓ increases. Specifically, if $V_\ell \propto M^{-\beta\ell}$ for $\beta > 0$, the number of samples N_ℓ required to estimate the ℓ -th correction term decreases with level ℓ , reducing the total computational cost.

To satisfy the variance decay condition $V_\ell \propto M^{-\beta\ell}$, we employ the synchronous coupling strategy of Shaw et al. (2025). Coarse and fine trajectories share a common Brownian motion realization, with coarse noise increments constructed as variance-preserving weighted sums of the corresponding fine increments. The correlation between coarse and fine trajectories ensures that the expected squared difference $\mathbb{E} \left[\|x_0^{(\ell)} - x_0^{(\ell-1)}\|^2 \right]$ decreases as $h_\ell \rightarrow 0$.

3.3.2. PROPOSAL DISTRIBUTION

The efficiency of our algorithm depends on the proposal distribution’s ability to generate particles in high-density regions of the conditional marginals $p_\theta(x_t | y)$. A simple choice is to employ the unconditional reverse kernel $r_t(x_t | x_{t+1}, y) = p_\theta(x_t | x_{t+1})$. Section 4 shows that this is effective for classification tasks with a small number of classes (e.g. MNIST, CIFAR-10; see Section 4.1) where the target distribution $p_\theta(x_t | y)$ constitutes a significant fraction of the probability mass generated by the unconditional proposal $p_\theta(x_t)$. This “high-overlap” regime ensures that the unconditional proposal generates particles within the effective support of the target with sufficiently high probability to maintain a healthy ESS.

However, considering the case where $p(y | x_0) \propto 1_{A_y}$, as $p_{t,\theta}(A_y) \downarrow 0$, choosing $r_t(x_t | x_{t+1}, y) = p_\theta(x_t | x_{t+1})$ will generate particle sets lying in low-probability regions of $p_\theta(x_t | y)$ with high probability. This can result in all unnormalized weights being very small at each timestep and with high probability the algorithm will fail to generate a single particle $x_0^{(i)}$ within the set A_y . In these regimes, our framework allows for targeted heuristics (e.g. TFG) to be used as the proposal r_t . The MLMC reweighting step

corrects the bias of these heuristics, ensuring asymptotically exact sampling. For higher dimensional problems, this can provide significant improvements (see Results).

3.3.3. SCHEDULE-BASED ADAPTIVE RESAMPLING

It is common in SMC algorithms to perform resampling only when the ESS drops below a predefined threshold (Del Moral et al., 2006), to reduce Monte Carlo variance. However, this adaptive resampling requires tracking the ESS, and thus calculating the weights, at each time step. In our setting, calculating the importance weights $w_t^{(i)}$ requires evaluating the MLMC estimator $\hat{p}_\theta(y | x_t)$. Performing this evaluation at every timestep $t \in \{1, \dots, T\}$ would be prohibitively expensive, dominating the cost of the algorithm.

Instead, we employ a fixed resampling schedule defined by a subset of timesteps $\mathcal{T} \subset \{1, \dots, T\}$. For a resampling step $\tau_k \in \mathcal{T}$, the sequential importance weight accumulates the discrepancies in both the likelihood and the transitions since the previous resampling step τ_{k-1} :

$$w_{\tau_k}^{(i)} = \frac{\hat{p}_\theta(y | x_{\tau_k}^{(i)})}{\hat{p}_\theta(y | x_{\tau_{k-1}}^{(i)})} \prod_{t=\tau_k}^{\tau_{k-1}-1} \frac{p_\theta(x_t | x_{t+1}^{(i)})}{r_{t+1}(x_t | x_{t+1}^{(i)}, y)}.$$

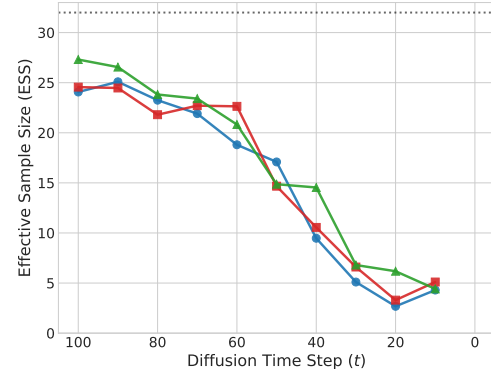
Thus we need only estimate the marginal likelihood at the resampling steps. When using the unconditional reverse process as the proposal distribution $r_t(x_t | x_{t+1}^{(i)}) = p_\theta(x_t | x_{t+1}^{(i)})$, the weight simplifies to the ratio of the estimated marginal likelihoods.

The choice of \mathcal{T} is motivated by the signal-to-noise dynamics of the diffusion process. In the early stages of the reverse process ($t \approx T$), the distribution of x_t is dominated by Gaussian noise. In this regime, the conditional likelihood $p_\theta(y | x_t)$ is approximately uniform across the particle set: since $\bar{\alpha}_t \approx 0$ for large t , the forward process has nearly erased dependence on x_0 , so $p_\theta(x_0 | x_t) \approx p_\theta(x_0)$ and thus $p_\theta(y | x_t) \approx p_\theta(y)$. As $t \rightarrow 0$, y contains more information about x_t and the variance of the likelihood weights increases in the absence of resampling, leading eventually to weight collapse.

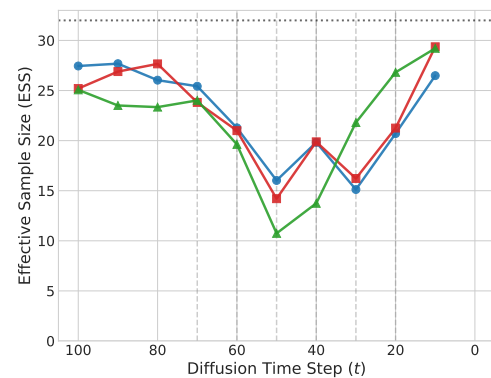
To balance particle diversity with computational cost, we choose \mathcal{T} to avoid resampling in the noise-dominated regime and concentrate resampling steps in the high-signal regime where particle degeneracy is of greater risk. For example, in image classification tasks (e.g. CIFAR-10), we find empirically that weight collapse is most severe in the interval $[70, 20]$. Prior to this window, weights are approximately uniform and thus resampling costs incur no benefit, whereas after this interval, images are mostly signal and $p_\theta(y | x_t)$ changes little as $x_t \rightarrow x_0$.

Of course, these boundaries will be problem-dependent. To estimate them for a new domain, we recommend an adaptive-

stepsize approach to monitoring the ESS of a pilot run—see Figure 2a. Obtaining an approximation of the optimal resampling window may save significant resources during subsequent runs of the sampling algorithm by focusing the resampling steps within the optimal time interval.



(a) ESS of 32 particles for three independent runs of CIFAR-10 classifier guidance without resampling.



(b) ESS of 32 particles for three independent runs of CIFAR-10 classifier guidance with resampling occurring at the dotted vertical lines.

Figure 2. We perform six independent runs of label guidance for CIFAR-10. In a), no resampling occurs and ESS begins to collapse at $t = 60$. In b), resampling occurs at $\{70, 60, 50, 40, 30\}$. The relevant window remains stable across runs, suggesting it can be identified with a single exploratory run.

3.4. Algorithm

The computational complexity of our algorithm is $O(N(T + |\mathcal{T}|ML))$, which can be decomposed into the cost of the proposal step $O(NT)$ and the reweighting $O(|\mathcal{T}|NML)$. The parameters $|\mathcal{T}|$ and L control the accuracy-cost trade-off, allowing practitioners to tune the algorithm to their requirements.

For practical deployment, the relevant metric is cost-per-success: the expected computational cost to generate at least one valid conditional sample. On CIFAR-10 (see Results),

Algorithm 1 SMC-MLMC for Training-Free Guidance

Require: Particles N , schedule \mathcal{T} , proposal r_t , likelihood estimator \hat{p} (MLMC)

- 1: **Init:** Sample $\{x_T^{(i)}\}_{i=1}^N \sim \mathcal{N}(0, I)$ and set prior likelihoods $\hat{L}^{(i)} \leftarrow 1$.
- 2: **for** $t = T$ **down to** 1 **do**
- 3: **Propagate:** Sample $x_{t-1}^{(i)} \sim r_t(x_{t-1} \mid x_t^{(i)}, y)$ for all $i \in \{1, \dots, N\}$.
- 4: **if** $t \in \mathcal{T}$ **then**
- 5: **Weight:** Compute $\hat{L}_{new}^{(i)} = \hat{p}(y \mid x_{t-1}^{(i)})$.
- 6: Calculate importance weights $w^{(i)}$.
- 7: **Resample:** Sample $\{x_{t-1}^{(i)}\}_{i=1}^N$ with replacement proportional to $\{w^{(i)}\}$.
- 8: **Update:** Set $\hat{L}^{(i)} \leftarrow \hat{L}_{new}^{(i)}$.
- 9: **end if**
- 10: **end for**
- 11: **return** $\{x_0^{(i)}\}_{i=1}^N$

our method achieves 95.6% accuracy with 23s per-run cost, requiring only a single run to generate a valid sample with high probability. In contrast, TFG-1 (52% accuracy, 13s) requires approximately 68.5 seconds for comparable success probability—thus our approach provides a **3× reduction** in cost. Similarly on ImageNet, our approach achieves a 58.3% success rate versus TFG’s 20.2%, translating to a **1.5× cost-per-success advantage** despite higher per-run cost.

By casting the problem in the framework of (unbiased) Monte Carlo approximation, our framework provides a principled path to achieving high success rates *efficiently*, through established variance reduction techniques: increasing the number of particles N , the frequency of resampling steps $|\mathcal{T}|$, and the number of MLMC samples L . Pure heuristic methods like DPS, which operate on single trajectories without resampling, offer no analogous mechanism for trading increased computation for improved accuracy. While TDS employs SMC and can eventually benefit from increased N , its reliance on biased likelihood approximations can lead to large distribution changes (and thus ESS collapse) along the path, resulting in poor sample complexity. In contrast, the weights in SMC-MLMC target the true conditional distributions $p_\theta(x_t \mid y)$, ensuring that the resampling schedule provides control over the magnitude of the distribution change at each step, which in turn controls the sample complexity of the algorithm (Marion et al., 2023a;b). This ability to increase accuracy by investing additional computation is particularly valuable for precision-critical applications in materials science, drug design, and scientific domains where generating valid samples is essential, even at increased computational cost.

4. Applications/Results

4.1. CIFAR-10

We evaluate SMC-MLMC on the CIFAR-10 (Krizhevsky & Hinton, 2009) label guidance problem. We use the CIFAR10-DDPM (Nichol & Dhariwal, 2021) as the pre-trained unconditional model. We set $T = 100$, $N = 16$, and use $r_t(x_t \mid x_{t+1}, y) = p_\theta(x_t \mid x_{t+1})$ as the proposal distribution. Likelihood estimation is performed via MLMC with $N_\ell = \{5, 2, 1\}$ for levels $\ell = 0, 1, 2$ respectively. We employ $|\mathcal{T}| = 4$ resampling steps at steps $\{60, 50, 40, 30\}$.

Table 1 compares our results against several state-of-the-art training-free guidance baselines (Ye et al., 2024). Algorithm 1 achieves a Top-1 Accuracy of 95.6%, outperforming the strongest heuristic baseline (Boosted TFG) by a margin of 18.5% and the standard DPS method by over 60.6%.

In addition to high validity, our method maintains high image fidelity, achieving an FID score of 46.3, comparable to the reference oracle (trained conditional diffusion model) (44.8) and a significant improvement over all training-free methods, including DPS (> 100) and LGD (100.0). These results indicate that SMC-MLMC significantly improves the fidelity of sampling from the target distribution. This is because the improved guidance approximation provides a smooth transition in the reverse distributions, enabling the resampling steps to effectively filter out degenerate particles without destroying the diversity required to approximate the data distribution.

Table 1. Comparison of SMC-MLMC ($N = 16$) against training-free guidance baselines (Ye et al., 2024) on the CIFAR-10 label guidance task. **Accuracy** is the fraction of generated samples classified as the target by an evaluation classifier separate from the guidance classifier. **Cost/Success** denotes the estimated time required to generate at least one valid sample with 95% confidence.

Method	Accuracy	FID	Cost/Success (s)
DPS	35.0%	> 100	—
LGD	50.0%	100.0	—
FreeDoM	62.0%	74.3	—
TFG-1	52.0%	91.7	68.5
TFG-4	77.1%	73.9	156.3
SMC-MLMC	95.6%	46.3	23.4

4.2. ImageNet

We also evaluated our approach on ImageNet 256×256 conditional generation using the pretrained Imagenet-DDPM (Dhariwal & Nichol, 2021). The higher dimensionality of ImageNet means that the unconditional reverse kernel $p_\theta(x_t \mid x_{t+1})$ is an inefficient proposal due to the vanishingly small volume of the target conditional support $p_\theta(x_t \mid y)$ (see Section 3.3.2). We therefore instead de-

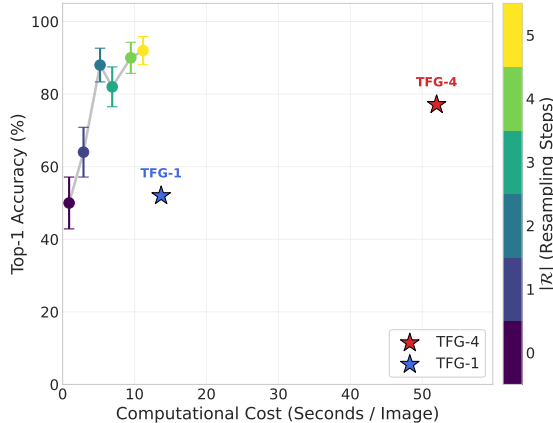


Figure 3. Computation cost versus accuracy of SMC-MLMC as a function of the number of resampling steps compared to TFG-1 and TFG-4 (Ye et al., 2024).

fine the proposal kernel $r_t(x_t | x_{t+1}, y)$ using the TFG-1 heuristic (Ye et al., 2024), leveraging the ability of TFG to steer particles toward candidate modes, while using our SMC-MLMC framework to correct the bias induced by the heuristic score approximation \tilde{s}_θ and ensuring the final particle set is sampled from the exact target distribution. This demonstrates the modularity of our framework: it can exploit biased heuristic guidance and, via reweighting, achieve success rates (50.5%) significantly higher than the heuristic alone (10.3%).

Results of our approach are shown in Table 2, compared to results obtained¹ by TFG-1 (Ye et al., 2024). Experiments are performed using $N = 4$, $T = 100$, and $\mathcal{T} = \{30\}$, with likelihood estimation by MLMC using $L = 2$ levels ($N_0 = 5$, $N_1 = 1$). All TFG hyperparameters follow the optimal settings reported in Ye et al. (2024). Across the six evaluated classes reported in Table 4, our algorithm achieves an average accuracy of 58.3%, nearly triple TFG’s average of 20.2%.

While SMC-MLMC incurs a higher per-run computational cost, its higher success rate gives it a lower improved

¹Results shown use the publicly released code from Ye et al. (2024) with parameter settings as reported there; however, our attempts to reproduce their results using their code yielded lower accuracy than originally reported. (It is possible this may be explained by differences in hardware or library versions.) Public comments on the Github package indicate that other users have similarly had difficulty reproducing the published accuracy; we contacted the authors without response. However, given that we compare SMC-MLMC using the TFG method as a proposal, vs the TFG method alone, this lower accuracy affects both. Since the magnitude of the accuracy improvement of SMC-MLMC over TFG on this problem (ImageNet) is comparable to that seen in Table 1 for CIFAR-10, which uses the authors’ own reported results, we believe this to be an accurate reflection of the relative improvement afforded by our approach.

Table 2. Aggregated performance on ImageNet 256×256 (Classes 111, 130, 207, 222, 333, 444).

Method	Success Rate	FID	Cost/Success (s)	Speedup
TFG (Baseline)	20.2%	231.9	230.0	1.0×
SMC-MLMC	58.3%	182.3	141.7	1.5×

cost-per-success, $\frac{2}{3}$ the cost of TFG. This efficiency advantage scales with task difficulty: on Class 333 (Hamster), where the baseline struggles with an 8% success rate, SMC-MLMC peaks at a $2.5\times$ efficiency gain. Additionally, SMC-MLMC improves average sample quality, reducing the FID from 231.9 to 182.3. These results suggest that SMC-MLMC is particularly valuable for difficult guidance tasks where heuristic methods struggle to generate accurate and diverse samples.

5. Conclusion

We have presented a principled Sequential Monte Carlo framework for training-free diffusion guidance. By replacing heuristic point estimates with unbiased Monte Carlo estimators of the marginal likelihood $p_\theta(y|x_t)$, our method eliminates the bias inherent in existing approaches and correctly captures the multimodality of the posterior distribution. Computational tractability is maintained by introduction of a Multilevel Monte Carlo (MLMC) estimator and a signal-adaptive resampling schedule. Empirical evaluation on CIFAR-10 demonstrates that this approach establishes a new state-of-the-art for training-free guidance, even surpassing the accuracy of training-based classifier guidance. Further results on ImageNet demonstrate the framework’s modularity: by employing existing heuristic methods (such as TFG) to form proposal distributions in the SMC framework, we achieve robust sampling in high-dimensional regimes where heuristics alone fail.

Posing the problem in this Monte Carlo approximation framework provides several avenues for additional/future refinement. Domain-specific proposal kernels $r_t(x_t|x_{t+1}, y)$ can be developed to further improve efficiency. Numerous other Monte Carlo variance-reduction techniques can be applied to the estimation of $p_\theta(y|x_t)$. Such advancements may be particularly valuable for constrained generation tasks in high-dimensions, such as the protein motif-scaffolding problem explored in Wu et al. (2023), extending the applicability of rigorous conditional sampling to complex scientific domains.

References

Bansal, A., Chu, H.-M., Schwarzschild, A., Sengupta, R., Goldblum, M., Geiping, J., and Goldstein, T. Universal guidance for diffusion models. In Kim, B., Yue, Y., Chaudhuri, S., Fragiadaki, K., Khan, M., and Sun, Y.

(eds.), *International Conference on Learning Representations*, volume 2024, pp. 51304–51323, 2024.

Blanchet, J. H., Glynn, P. W., and Pei, Y. Unbiased multilevel Monte Carlo: Stochastic optimization, steady-state simulation, quantiles, and other applications. *ArXiv preprint*, abs/1904.09929, 2019.

Cardoso, G., el idrissi, Y. J., Corff, S. L., and Moulines, E. Monte carlo guided denoising diffusion models for bayesian linear inverse problems. In *The Twelfth International Conference on Learning Representations*, 2024.

Chatterjee, S. and Diaconis, P. The sample size required in importance sampling. *The Annals of Applied Probability*, 28(2):1099 – 1135, 2018. doi: 10.1214/17-AAP1326.

Chung, H., Kim, J., Mccann, M. T., Klasky, M. L., and Ye, J. C. Diffusion posterior sampling for general noisy inverse problems. In *The Eleventh International Conference on Learning Representations*, 2023.

Del Moral, P., Doucet, A., and Jasra, A. Sequential Monte Carlo Samplers. *Journal of the Royal Statistical Society Series B: Statistical Methodology*, 68(3):411–436, 05 2006. ISSN 1369-7412. doi: 10.1111/j.1467-9868.2006.00553.x.

Dhariwal, P. and Nichol, A. Q. Diffusion models beat GANs on image synthesis. In Beygelzimer, A., Dauphin, Y., Liang, P., and Vaughan, J. W. (eds.), *Advances in Neural Information Processing Systems*, 2021.

Giles, M. B. Multilevel Monte Carlo path simulation. *Operations Research*, 56(3):607–617, 2008. doi: 10.1287/opre.1070.0496.

Ho, J. and Salimans, T. Classifier-free diffusion guidance. *ArXiv preprint*, abs/2207.12598, 2022.

Ho, J., Jain, A., and Abbeel, P. Denoising diffusion probabilistic models. In Larochelle, H., Ranzato, M., Hadsell, R., Balcan, M., and Lin, H. (eds.), *Advances in Neural Information Processing Systems 33: Annual Conference on Neural Information Processing Systems 2020, NeurIPS 2020, December 6-12, 2020, virtual*, 2020.

Hoogeboom, E., Satorras, V. G., Vignac, C., and Welling, M. Equivariant diffusion for molecule generation in 3D. In Chaudhuri, K., Jegelka, S., Song, L., Szepesvari, C., Niu, G., and Sabato, S. (eds.), *Proceedings of the 39th International Conference on Machine Learning*, volume 162 of *Proceedings of Machine Learning Research*, pp. 8867–8887. PMLR, 17–23 Jul 2022.

Kong, Z., Ping, W., Huang, J., Zhao, K., and Catanzaro, B. Diffwave: A versatile diffusion model for audio synthesis. In *International Conference on Learning Representations*, 2021.

Krizhevsky, A. and Hinton, G. Learning multiple layers of features from tiny images, 2009.

Li, X., Thickstun, J., Gulrajani, I., Liang, P. S., and Hashimoto, T. B. Diffusion-lm improves controllable text generation. In Koyejo, S., Mohamed, S., Agarwal, A., Belgrave, D., Cho, K., and Oh, A. (eds.), *Advances in Neural Information Processing Systems*, volume 35, pp. 4328–4343. Curran Associates, Inc., 2022.

Lugmayr, A., Danelljan, M., Romero, A., Yu, F., Timofte, R., and Van Gool, L. Repaint: Inpainting using denoising diffusion probabilistic models. In *Proceedings of the IEEE/CVF Conference on Computer Vision and Pattern Recognition (CVPR)*, pp. 11461–11471, June 2022.

Marion, J., Mathews, J., and Schmidler, S. C. Finite-sample complexity of sequential Monte Carlo estimators. *The Annals of Statistics*, 51(3):1357 – 1375, 2023a. doi: 10.1214/23-AOS2295.

Marion, J., Mathews, J., and Schmidler, S. C. Finite sample L_2 bounds for sequential Monte Carlo and adaptive path selection. *arXiv:1807.01346 [stat.CO]*, 2023b.

Nichol, A. Q. and Dhariwal, P. Improved denoising diffusion probabilistic models. In Meila, M. and Zhang, T. (eds.), *Proceedings of the 38th International Conference on Machine Learning*, volume 139 of *Proceedings of Machine Learning Research*, pp. 8162–8171. PMLR, 18–24 Jul 2021.

Paszke, A., Gross, S., Massa, F., Lerer, A., Bradbury, J., Chanan, G., Killeen, T., Lin, Z., Gimelshein, N., Antiga, L., Desmaison, A., Kopf, A., Yang, E., DeVito, Z., Raison, M., Tejani, A., Chilamkurthy, S., Steiner, B., Fang, L., Bai, J., and Chintala, S. Pytorch: An imperative style, high-performance deep learning library. In Wallach, H. M., Larochelle, H., Beygelzimer, A., d’Alché-Buc, F., Fox, E. B., and Garnett, R. (eds.), *Advances in Neural Information Processing Systems 32: Annual Conference on Neural Information Processing Systems 2019, NeurIPS 2019, December 8-14, 2019, Vancouver, BC, Canada*, pp. 8024–8035, 2019.

Rombach, R., Blattmann, A., Lorenz, D., Esser, P., and Ommer, B. High-resolution image synthesis with latent diffusion models. In *Proceedings of the IEEE/CVF Conference on Computer Vision and Pattern Recognition (CVPR)*, pp. 10684–10695, June 2022.

Rubin, D. B. The calculation of posterior distributions by data augmentation: Comment: A noniterative sampling/importance resampling alternative to the data augmentation algorithm for creating a few imputations when fractions of missing information are modest: The SIR algorithm. *Journal of the American Statistical Association*, 82(398):543–546, 1987. ISSN 01621459, 1537274X.

Shaw, L., Haji-Ali, A.-L., Pereyra, M., and Zygalakis, K. Bayesian computation with generative diffusion models by multilevel monte carlo. *Philosophical Transactions of the Royal Society A: Mathematical, Physical and Engineering Sciences*, 383(2299):20240333, 06 2025. ISSN 1364-503X. doi: 10.1098/rsta.2024.0333.

Sohl-Dickstein, J., Weiss, E. A., Maheswaranathan, N., and Ganguli, S. Deep unsupervised learning using nonequilibrium thermodynamics. In Bach, F. R. and Blei, D. M. (eds.), *Proceedings of the 32nd International Conference on Machine Learning, ICML 2015, Lille, France, 6-11 July 2015*, volume 37 of *JMLR Workshop and Conference Proceedings*, pp. 2256–2265. JMLR.org, 2015.

Song, J., Zhang, Q., Yin, H., Mardani, M., Liu, M.-Y., Kautz, J., Chen, Y., and Vahdat, A. Loss-guided diffusion models for plug-and-play controllable generation. In Krause, A., Brunskill, E., Cho, K., Engelhardt, B., Sabato, S., and Scarlett, J. (eds.), *Proceedings of the 40th International Conference on Machine Learning*, volume 202 of *Proceedings of Machine Learning Research*, pp. 32483–32498. PMLR, 2023.

Song, Y. and Ermon, S. Generative modeling by estimating gradients of the data distribution. In Wallach, H. M., Larochelle, H., Beygelzimer, A., d’Alché-Buc, F., Fox, E. B., and Garnett, R. (eds.), *Advances in Neural Information Processing Systems 32: Annual Conference on Neural Information Processing Systems 2019, NeurIPS 2019, December 8-14, 2019, Vancouver, BC, Canada*, pp. 11895–11907, 2019.

Song, Y., Sohl-Dickstein, J., Kingma, D. P., Kumar, A., Ermon, S., and Poole, B. Score-based generative modeling through stochastic differential equations. In *9th International Conference on Learning Representations, ICLR 2021, Virtual Event, Austria, May 3-7, 2021*. OpenReview.net, 2021.

Trippé, B. L., Yim, J., Tischer, D., Baker, D., Broderick, T., Barzilay, R., and Jaakkola, T. S. Diffusion probabilistic modeling of protein backbones in 3D for the motif-scaffolding problem. In *The Eleventh International Conference on Learning Representations*, 2023.

Whiteley, N. and Lee, A. Twisted particle filters. *The Annals of Statistics*, 42(1):115 – 141, 2014. doi: 10.1214/13-AOS1167.

Wu, L., Trippé, B., Naesseth, C., Blei, D., and Cunningham, J. P. Practical and asymptotically exact conditional sampling in diffusion models. In Oh, A., Naumann, T., Globerson, A., Saenko, K., Hardt, M., and Levine, S. (eds.), *Advances in Neural Information Processing Systems*, volume 36, pp. 31372–31403. Curran Associates, Inc., 2023.

Ye, H., Lin, H., Han, J., Xu, M., Liu, S., Liang, Y., Ma, J., Zou, J., and Ermon, S. TFG: Unified training-free guidance for diffusion models. In Globerson, A., Mackey, L., Belgrave, D., Fan, A., Paquet, U., Tomczak, J., and Zhang, C. (eds.), *Advances in Neural Information Processing Systems*, volume 37, pp. 22370–22417. Curran Associates, Inc., 2024. doi: 10.5220/079017-0704.

Yu, J., Wang, Y., Zhao, C., Ghanem, B., and Zhang, J. Freedom: Training-free energy-guided conditional diffusion model. In *Proceedings of the IEEE/CVF International Conference on Computer Vision (ICCV)*, pp. 23174–23184, October 2023.

A. Gaussian Mixture Models

A.1. Forward Process Marginal Distributions

Suppose $x \in \mathbb{R}^d$ is distributed according to a GMM with K components. We have $p_0(x|y=k) = N(x; \mu_k, \sigma_0^2 I)$ and, assuming equal component weights, $p_0(x) = \frac{1}{K} \sum_{k=1}^K N(x; \mu_k, \sigma_0^2 I)$.

Consider the forward process conditioned on $y = k$; so x_0 is drawn from component k . At time t we have $x_t = \sqrt{\bar{\alpha}_t} x_0 + \epsilon_t$ where $\epsilon_t \sim N(0, (1 - \bar{\alpha}_t)I)$ so

$$\begin{aligned}\mu_{k,t} &:= \mathbb{E}[x_t | y = k] = \sqrt{\bar{\alpha}_t} \mu_k \\ \sigma_t^2 &:= \text{Cov}[x_t | y = k] = \bar{\alpha}_t \sigma_0^2 I + (1 - \bar{\alpha}_t)I = (1 - \bar{\alpha}_t(1 - \sigma_0^2))I.\end{aligned}$$

Then the marginal distribution of the forward process at time t is also a GMM:

$$q_t(x_t) = \frac{1}{K} \sum_{k=1}^K N(x_t; \mu_{k,t}, \sigma_t^2 I)$$

and the membership probabilities are straightforward to calculate:

$$\Pr(y = k | x_t) = \frac{N(x_t; \mu_{k,t}, \sigma_t^2 I)}{\sum_{j=1}^K N(x_t; \mu_{j,t}, \sigma_t^2 I)} = \frac{\exp\left(-\frac{\|x_t - \mu_{k,t}\|^2}{2\sigma_t^2}\right)}{\sum_{j=1}^K \exp\left(-\frac{\|x_t - \mu_{j,t}\|^2}{2\sigma_t^2}\right)}.$$

A.2. DPS estimation bias

When $K = 2$ we can use Jensen's inequality to show that DPS overestimates $p(y | x_t)$. Let $\mu_1 = \mu$ and $\mu_2 = -\mu$. We can rewrite the membership probability as

$$\Pr(y = 1 | x_t) = \frac{1}{1 + \exp\left(\frac{-2x_t^\top \mu}{\sigma_t^2}\right)}.$$

When $\frac{2x_t^\top \mu}{\sigma_t^2} > 0$ (implying $p(y = 1 | x_t) > 0.5$, this function is strictly concave. Thus, by Jensen's inequality we have

$$p(y = 1 | x_t) = \mathbb{E}_{x_0 \sim p(x_0 | x_t)}[p(y = 1 | x_0)] < p(y = 1 | \mathbb{E}_{x_0 \sim p(x_0 | x_t)}[x_0]).$$

Therefore, in regions where $p(y = 1 | x_t) > 0.5$, the DPS estimate will overestimate the class membership probability. By the same argument, when $p(y = 1 | x_t) < 0.5$ (or $\frac{2x_t^\top \mu}{\sigma_t^2} < 0$) the DPS estimate is strictly less than the class membership probability. Because equality holds only when $x_t^\top \mu = 0$, a hyperplane of measure zero, we have

$$P_{x_t}(\tilde{p}(y | x_t) \neq p_\theta(y | x_t)) = 1.$$

A.3. Gaussian Likelihoods

Assume $K = 2$ with $\mu_1 = \mu$, $\mu_2 = -\mu$, and isotropic variance $\sigma_0^2 I$ for each mode. To ensure that the modes remain distinguishable as dimension increases, take the signal to noise ratio to be constant with $d: \|\mu\|^2 = c \cdot d$ for some constant $c > 0$. For large t , we will have

$$\hat{x}_0(x_t) = \mathbb{E}[x_0 | x_t] \approx 0.$$

Consider a Gaussian likelihood centered at μ_1 $p(y | x) \propto \exp\left(-\frac{\|x - \mu\|^2}{2\omega^2}\right)$ as is typical in diffusion guidance problems. Evaluating this at the point estimate gives

$$p(y | \hat{x}_0(x_t)) \propto \exp\left(-\frac{cd}{2\omega^2}\right)$$

B. Experiment Details

B.1. CIFAR-10 Experiment Details

Diffusion Model. We use the pretrained DDPM checkpoint from `google/ddpm-cifar10-32` via the HuggingFace Diffusers library. The model operates on 32×32 RGB images with $T = 100$ diffusion steps (mapped to the model’s 1000-step schedule via stride 10).

Classifier. For guidance, we use a pretrained ResNet-34 classifier (`resnet34_cifar10`) from the `timm` library. Images are normalized using CIFAR-10 statistics ($\mu = [0.491, 0.482, 0.447]$, $\sigma = [0.202, 0.199, 0.201]$). For evaluation, we use a separate ConvNeXT-Tiny classifier to avoid overfitting to the guidance signal.

SMC Configuration. We use $N = 16$ particles per chain. Resampling occurs at timesteps $\mathcal{T} = \{60, 50, 40, 30\}$ (i.e., $|\mathcal{T}| = 4$ in the reported experiments). Resampling is triggered when ESS falls below $0.5N$.

MLMC Configuration. The base integrator uses $T_0 = 16$ steps. We use $L = 3$ levels with sample counts $N_\ell = \{5, 2, 1\}$ for levels $\ell = 0, 1, 2$ respectively. Coupled trajectories follow Algorithm 2 of [Shaw et al. \(2025\)](#).

Evaluation. For each of the 10 CIFAR-10 classes, we generate 2,000 samples (20 parallel jobs \times 100 samples each). FID is computed against class-filtered reference images from the CIFAR-10 test set.

B.2. ImageNet Experiment Details

Diffusion Model. We use the pretrained 256×256 unconditional ImageNet diffusion model from [Dhariwal & Nichol \(2021\)](#), with checkpoint `openai_imagenet.pt`. We use $T = 100$ inference steps (subsampled from 1000 training steps) with DDIM sampling ($\eta = 1.0$).

Classifier. For guidance, we use a pretrained Vision Transformer (`google/vit-base-patch16-224`) from HuggingFace. For evaluation, we use a separate DeiT-Small model (`facebook/deit-small-patch16-224`).

Proposal Distribution. Unlike CIFAR-10, the unconditional reverse kernel is insufficient for ImageNet due to the large state space. We therefore use TFG ([Ye et al., 2024](#)) as the proposal distribution $r_t(x_{t-1}|x_t, y)$.

SMC Configuration. We use $N = 4$ particles per chain with resampling at timestep $\mathcal{T} = \{30\}$ (i.e., $|\mathcal{T}| = 1$). Resampling is triggered when ESS falls below $N/2 = 2$.

MLMC Configuration. We use $L = 2$ levels with sample counts $N_\ell = \{5, 1\}$ for levels $\ell = 0, 1$. The base integrator uses $T_0 = 16$ steps for $t > 50$, reducing to $T_0 = 4$ steps for $t \leq 50$ (dynamic schedule).

Evaluation. We evaluate on 6 ImageNet classes (111, 130, 207, 222, 333, 444) with 200 samples per class. Success rate is computed as the fraction of runs producing at least one correctly classified particle.

B.3. Hardware and Software

All experiments were run using PyTorch ([Paszke et al., 2019](#)). We used the HuggingFace library for to implement the CIFAR-10 experiments as well as details from the code released by the authors of [Wu et al. \(2023\)](#). We relied heavily on the code released in conjunction with [Ye et al. \(2024\)](#) for our ImageNet experiments.

The CIFAR-10 experiments were run on NVIDIA RTX 5000 Ada GPUs with 32GB memory. ImageNet experiments were run using NVIDIA H200 GPUs. We estimate 100 GPU hours for the H200s and 50 GPU hours for the RTX 5000s.

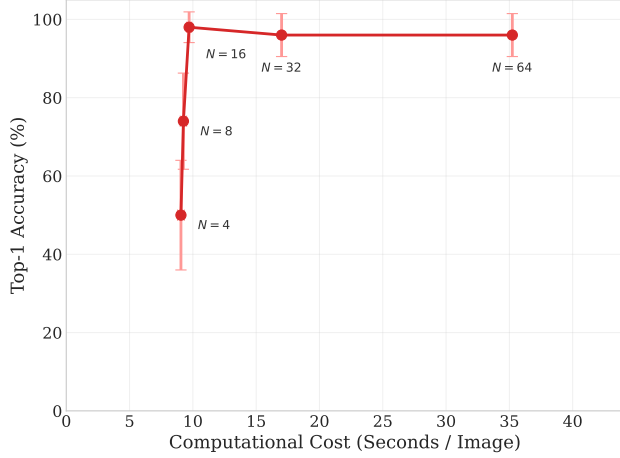


Figure 4. Computation cost versus accuracy of SMC-MLMC as a function of number of particles N for CIFAR-10.

C. Expanded Results

C.1. CIFAR-10

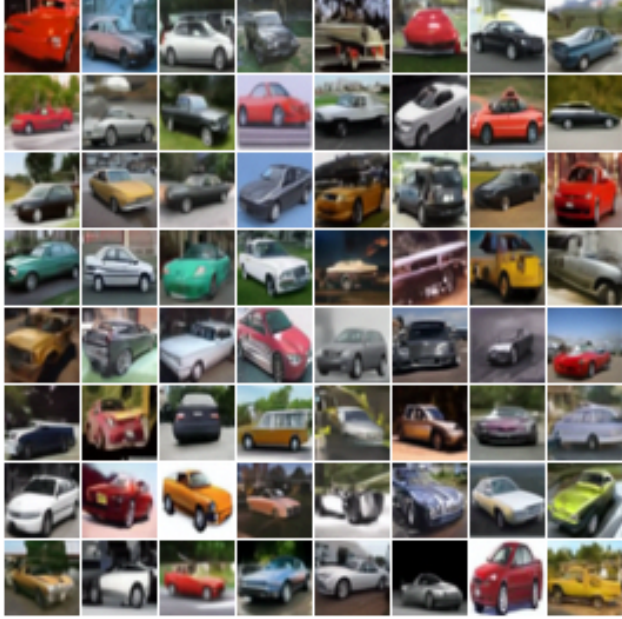
Ablation Studies In Figure 4 we show computational cost versus accuracy for a variety of particle sizes N on the CIFAR-10 label guidance task.

Per-Class Results We provide the per-class accuracy and FID for SMC-MLMC in Table 3.

Table 3. Per-class breakdown of SMC-MLMC performance on CIFAR-10 conditional generation.

Target Class	Top-1 Accuracy	FID
Airplane	94.9%	54.8
Automobile	97.6%	35.0
Bird	94.3%	51.0
Cat	92.7%	61.1
Deer	96.1%	39.0
Dog	91.3%	60.2
Frog	99.2%	47.6
Horse	95.6%	37.3
Ship	96.6%	43.2
Truck	98.2%	34.1
Average	95.6%	46.3

Qualitative Comparison Figure 5 presents 64 CIFAR-10 automobiles generated by SMC-MLMC and TFG-4, selected at random. SMC-MLMC consistently generates higher quality, more realistic images than TFG-4.



(a) SMC-MLMC



(b) TFG-4

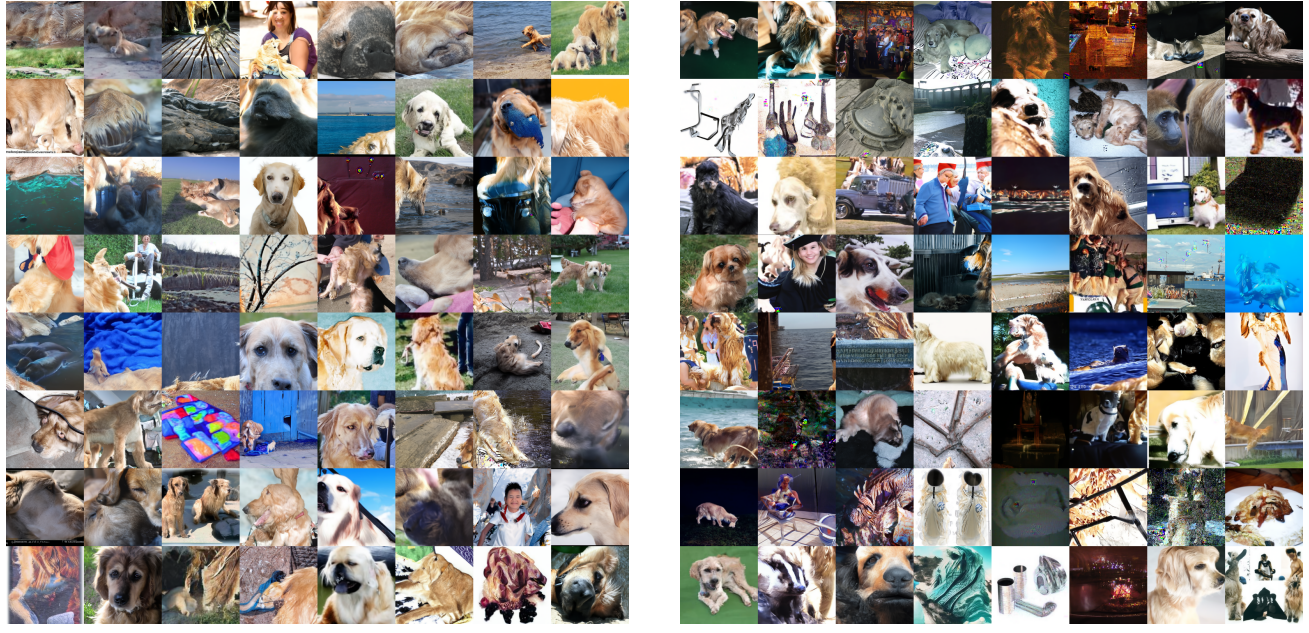
Figure 5. Qualitative comparison of CIFAR10 automobiles generated by (a) SMC-MLMC and (b) TFG-4 (Ye et al., 2024).

C.2. ImageNet Qualitative Comparison

Figure 6 presents randomly selected ImageNet images generated by SMC-MLMC and TFG-1 for comparison. We see a higher frequency of the target class (207, golden retriever) in (a) SMC-MLMC.

C.3. ImageNet Per-Class Results

Table 4 provides per-class results for the ImageNet experiments.



(a) SMC-MLMC

(b) TFG-1

Figure 6. Qualitative comparison of ImageNet golden retrievers (class 207) by (a) SMC-MLMC and (b) TFG-1 (Ye et al., 2024).

Table 4. Per-class SMC-MLMC performance on ImageNet compared to TFG Ye et al. (2024).

Target Class	Method	Success Rate	FID ↓	Runtime (s)	Cost/Success (s)
111 (Nematode)	TFG (Baseline)	41.0%	199.5	12	72
	SMC-MLMC	71.0%	204.6	34	102
130 (Flamingo)	TFG (Baseline)	20.0%	243.0	12	168
	SMC-MLMC	56.5%	167.9	34	136
207 (Golden Retriever)	TFG (Baseline)	28.0%	207.3	12	120
	SMC-MLMC	74.5%	143.4	34	102
222 (Kuvasz)	TFG (Baseline)	13.9%	232.0	12	252
	SMC-MLMC	51.0%	199.5	34	170
333 (Hamster)	TFG (Baseline)	8.0%	235.1	12	432
	SMC-MLMC	48.5%	178.0	34	170
444 (Tandem Bicycle)	TFG (Baseline)	10.3%	274.4	12	336
	SMC-MLMC	48.3%	200.6	34	170